CONFIDENTIAL

Copy
RM L9H22

NACA RM L9H22

NACA

RESEARCH MEMORANDUM

AERODYNAMIC CHARACTERISTICS OF A WING WITH UNSWEPT QUARTER-CHORD LINE, ASPECT RATIO 4, TAPER RATIO 0.6, AND NACA 65A006 AIRFOIL SECTION

TRANSONIC-BUMP METHOD

By Kenneth W. Goodson and William D. Morrison, Jr.

Langley Aeronautical Laboratory
Langley Air Force Base, Va.

NATIONAL ADVISORY COMMITTEE FOR AERONAUTICS

WASHINGTON

October 21, 1949

CONFIDENTIAL

NATIONAL ADVISORY COMMITTEE FOR AERONAUTICS

RESEARCH MEMORANDUM

AERODYNAMIC CHARACTERISTICS OF A WING WITH UNSWEPT QUARTER-CHORD LINE, ASPECT RATIO 4, TAPER RATIO 0.6, AND NACA 65A006 AIRFOIL SECTION

TRANSONIC-BUMP METHOD

By Kenneth W. Goodson and William D. Morrison, Jr.

SUMMARY

As part of an NACA transonic research program, a series of wing-body combinations are being investigated in the Langley high-speed 7- by 10-foot tunnel over a Mach number range of 0.60 to 1.18 utilizing the transonic-bump technique.

This paper presents the results of the investigation of a wing alone and a wing-fuselage combination employing a wing with an unswept quarter-chord line, aspect ratio 4, taper ratio 0.6, and an NACA 65A006 airfoil section. Lift, drag, pitching moment, and root bending moment were obtained for these configurations. Effective downwash angles and dynamic-pressure characteristics were also obtained for these configurations for a range of tail heights in the region of a probable tail location. In order to expedite publishing these data, only a brief analysis is included.

INTRODUCTION

A series of wings is being investigated in the Langley high-speed 7- by 10-foot tunnel to study the effects of wing geometry on the wing-alone and wing-fuselage longitudinal stability characteristics at transonic speeds. The same fuselage is being used for all wings tested in this series. A Mach number range between 0.60 and 1.18 is obtained by utilizing the transonic-bump technique.

This paper presents the results of the investigation of the wing–alone and of the wing–fuselage configurations employing a wing with an unswept quarter–chord line, aspect ratio 4, taper ratio 0.6, and an NACA 65A006 airfoil section parallel to the air stream. The results of closely related sweptback–wing investigations, which are part of the present transonic program, are presented in references 1 to 3.

MODEL AND APPARATUS

The wing of the semispan model had 0° of sweepback referred to the quarter–chord line, a taper ratio of 0.60, an aspect ratio of 4, and an NACA 65A006 airfoil section parallel to the free stream. The wing was made of beryllium copper and the fuselage of brass. A two–view drawing of the model is presented in figure 1, and ordinates of the fuselage of fineness ratio 10 can be found in table I.

The model was mounted on an electrical strain–gage balance enclosed in the bump, and the lift, drag, pitching moment, and bending moment about the model plane of symmetry were measured with potentiometers.

Effective downwash angles were determined for a range of tail heights by measuring the floating angles of free–floating tails with the aid of calibrated galvanometers. Details of the floating tails are shown in figures 2 and 3, and a pictorial view of the model on the bump, showing three of the floating tails, is given in figure 4. The tails used in this investigation were of the same geometry as those used in references 1 to 3. A pictorial view of the sponge wiper seal installed on the model is shown in figure 5.

A total–pressure rake was employed to determine point dynamic–pressure ratios for a range of tail heights in a plane which contained the 25–percent–mean–aerodynamic–chord point of the free–floating tails. The total–pressure tubes were spaced 1/8 inch apart near the wing chord line extended and 1/4 inch apart elsewhere.

A few surveys were also made in a spanwise plane at the same longitudinal location as the previously discussed surveys. The rake utilized for these additional surveys had a tube spacing of 1/4 inch.

SYMBOLS

C_L lift coefficient $\left(\frac{\text{Twice panel lift}}{qS}\right)$

C_D drag coefficient $\left(\frac{\text{Twice panel drag}}{qS}\right)$

C_m pitching-moment coefficient referred to $0.25\bar{c}$ $\left(\frac{\text{Twice panel pitching moment}}{qS\bar{c}}\right)$

C_B bending-moment coefficient at plane of symmetry $\left(\frac{\text{Root bending moment}}{q\frac{S}{2}\frac{b}{2}}\right)$

q effective dynamic pressure over span of model, pounds per square foot $\left(\frac{1}{2}\rho V^2\right)$

S twice wing area of semispan model, 0.125 square foot

$\bar{c}$ mean aerodynamic chord of wing, 0.181 foot; based on relationship $\frac{2}{S}\int_0^{b/2} c^2 dy$ (using theoretical tip)

c local wing chord

b twice span of semispan model

y spanwise distance from plane of symmetry

ρ air density, slugs per cubic foot

V airspeed, feet per second

M effective Mach number over span of model

M_l local Mach number

M_a average chordwise local Mach number

R Reynolds number of wing based on $\bar{c}$

α angle of attack, degrees

ϵ effective downwash angle, degrees

q_{wake}/q ratio of point dynamic pressure to free-stream dynamic pressure

y_{cp} lateral center of pressure, percent semispan $\left(\frac{100C_B}{C_L}\right)$

h_t tail height relative to wing chord plane extended, percent semispan, positive for tail positions above chord plane extended

TESTS

The tests were made in the Langley high-speed 7- by 10-foot tunnel utilizing an adaptation of the NACA wing-flow technique for obtaining transonic speeds. The technique used involves placing the model in the high-velocity flow field generated over the curved surface of a bump on the tunnel floor. (See reference 4.)

Typical contours of local Mach number in the vicinity of the model location on the bump, obtained from surveys with no model in position, are shown in figure 6. It is seen that there is a Mach number variation of about 0.05 over the model semispan at low Mach numbers and from 0.07 to 0.08 at the higher Mach numbers. The chordwise Mach number variation is generally less than 0.01. No attempt has been made to evaluate the effects of this chordwise and spanwise Mach number variation. Note that the long-dashed lines shown near the root of the wing (fig. 6) represent a local Mach number 5 percent below the maximum value and indicate the extent of the bump boundary layer. The effective test Mach number was obtained from contour charts similar to those presented in figure 6 using the relationship

$$M = \frac{2}{S}\int_0^{b/2} cM_a \, dy$$

The variation of mean test Reynolds number with Mach number is shown in figure 7. The boundaries in the figure indicate the range in Reynolds number caused by variations in atmospheric test conditions in the course of the investigation.

Force and moment data, effective downwash angles, and the ratio of dynamic pressure at 25 percent of the mean aerodynamic chord of the free-floating tails to free-stream dynamic pressure were obtained for the model wing-alone and wing-fuselage configurations tested through a Mach number range of 0.60 to 1.18 and an angle-of-attack range of -2° to 12°. A few surveys were also made to determine the spanwise variation of wake dynamic pressure at a Mach number of 1.10.

The end-plate tare corrections to the drag and to the downwash data were obtained through the test Mach number range at 0° angle of attack by testing the model configurations without end plates. A gap of about 1/16 inch was maintained between the wing root chord and the bump surface, and a sponge wiper seal was fastened to the wing butt beneath the surface of the bump to minimize leakage. The end-plate tares were assumed to be constant with angle of attack, and the tares obtained at zero angle of attack were applied to all drag and downwash data. Jet-boundary corrections have not been evaluated because the boundary conditions to be satisfied are not rigorously defined. However, inasmuch as the effective flow field is large compared with the span and chord of the model, the corrections are believed to be small. No base-pressure correction has been applied to the wing-fuselage drag data.

By measuring tail floating angles without a model installed, it was determined that a tail spacing of 2 inches would produce negligible interference effects of reflected shock waves on the tail floating angles. Downwash angles for the wing-alone configuration were therefore obtained simultaneously for the middle, highest, and lowest tail positions in one series of tests and simultaneously for the two intermediate positions in succeeding runs. (See fig. 3.) For the wing-fuselage tests, the effective downwash angles at the chord plane extended were determined by mounting a free-floating tail on the center line of the fuselage. The downwash angles presented are increments from the tail floating angles without a model in position. It should be noted that the

floating angles measured are a measure of the angle-of-zero pitching moment about the tail pivot axis rather than the angle-of-zero lift. It has been estimated, however, that for this tail arrangement a downwash gradient as large as 2° across the span of the tail will result in an error of less than 0.2° in the measured downwash angle.

The total-pressure readings were obtained at constant angles of attack through the Mach number range without an end plate on the model to eliminate end-plate wakes and with the support-strut gap sealed with a rubber sponge seal to minimize any strut-leakage effects. The static-pressure values used in computing the dynamic-pressure ratios were obtained by use of a static probe with no model in position.

RESULTS AND DISCUSSION

A table of the figures presenting the results follows:

The discussion is based on the summarized values given in figure 15 unless otherwise noted. The slopes summarized in figure 15 have been averaged over a lift-coefficient range of ± 0.1.

Lift and Drag Characteristics

The isolated-wing lift-curve slope measured near zero lift was about 0.074 at a Mach number of 0.60. This value compares favorably with a value of 0.073 estimated for this Mach number using unpublished semispan data for a geometrically similar model from the Langley two-dimensional low-turbulence tunnel ($R = 3.0 \times 10^6$ to 12.0×10^6) as a low-speed point and applying a compressibility correction as outlined in reference 5. The peak lift-curve slope occurred at about $M = 0.87$ with a secondary peak at $M = 1.03$. The addition of the fuselage generally had only a slight effect on the lift-curve slope, although the peak lift-curve slope was delayed to a Mach number of about 0.92.

Drag rise at zero lift began at a Mach number of about 0.87 for both the wing–alone and wing–fuselage configurations.

The lateral center of pressure for the wing alone was located at 42 percent of the semispan at a Mach number of 0.60 at lift coefficients below 0.5. The same lateral center–of–pressure location was obtained at low speed and high Reynolds numbers in the Langley two–dimensional low–turbulence tunnel for a geometrically similar model. The lateral center of pressure gradually moved outboard as the subsonic speeds increased and was located at about 44.5 percent of the semispan at $M = 0.98$. Between $M = 0.98$ and 1.05 there was a fairly abrupt inboard movement of y_{cp} to 41 percent of the semispan and this value remained about constant up to $M = 1.18$. The addition of the fuselage moved y_{cp} inboard from 1 to 2 percent of the semispan through the Mach number range.

Pitching–Moment Characteristics

Near the zero lift coefficient the wing–alone aerodynamic center was located at about 24 percent of the mean aerodynamic chord $\left(\left(\frac{\partial C_m}{\partial C_L}\right)_M = 0.01\right)$ at low Mach numbers. The aerodynamic center moved forward about 3 percent of the mean aerodynamic chord as the Mach number was increased to 0.84. In the speed range between $M = 0.84$ and 1.03 the aerodynamic center moved back to about 37 percent mean aerodynamic chord and thereafter remained about constant up to $M = 1.18$. The addition of the fuselage moved the aerodynamic center forward about 7 percent mean aerodynamic chord at the lower Mach numbers and from 4 to 5 percent forward at Mach numbers above unity. By using the theoretical methods of reference 6, it was estimated that the fuselage would move the wing–alone aerodynamic center forward about 6 percent mean aerodynamic chord at low subsonic speeds.

Downwash and Dynamic–Pressure Surveys

The downwash gradient $d\epsilon/d\alpha$ near zero lift for the wing alone was a maximum slightly above the chord plane extended throughout the Mach number range. (See fig. 12.) The variation of $d\epsilon/d\alpha$ with Mach number for tail positions of 0 and 30 percent of the semispan above and below the chord line extended was quite similar to the lift–curve–slope variation with Mach number in that a double peaking was present at about the same Mach numbers. (See fig. 15.) Between the peak values of downwash gradient which occurred at $M = 0.90$ and 1.02, a rather rapid variation of $d\epsilon/d\alpha$ with Mach number is

indicated. When the fuselage was added to the isolated wing these large changes in downwash slope were not evident.

The results of the point dynamic-pressure surveys made in a vertical plane containing the 25-percent-mean-aerodynamic-chord point of the free-floating tails used in the downwash surveys are presented in figure 13. Below a Mach number of 0.95 there is very little difference in the wake characteristics of the wing-alone and wing-fuselage configurations except that larger wake losses are indicated at $\alpha = 10^{\circ}$ for the wing-fuselage condition because of a more fully developed stall. At the Mach numbers above 1.00 at moderate and high angles of attack, however, the wake associated with the wing-fuselage configuration was much more extensive than the corresponding isolated-wing wake (fig. 13). In order to gain further information concerning the possible cause of these wake differences, a few spanwise surveys were made at the same tail length used for the vertical surveys. The results of these additional surveys (fig. 14) indicated that, although the isolated-wing wake losses are practically constant along the span of the tail, a very large spanwise dynamic-pressure gradient was present near the fuselage. The flagged symbols plotted in figure 14 represent the data obtained from figure 13 for the same survey location. It is apparent from the comparison of the two sets of data that, while the wake measurements behind the wing alone could be repeated, the wake characteristics behind the wing-fuselage combination could not be repeated. These discrepancies in wake behavior as well as the steep gradient in dynamic pressure close to the wing-fuselage juncture may be attributable to unsteady flow conditions induced by shock formations and separation at the wing-fuselage juncture.

Langley Aeronautical Laboratory
National Advisory Committee for Aeronautics
Langley Air Force Base, Va.

REFERENCES

1. Weil, Joseph, and Goodson, Kenneth W.: Aerodynamic Characteristics of a Wing with Quarter-Chord Line Swept Back 45°, Aspect Ratio 4, Taper Ratio 0.6, and NACA 65A006 Airfoil Section. Transonic-Bump Method. NACA RM L9A21, 1949.

2. Sleeman, William C., Jr., and Becht, Robert E.: Aerodynamic Characteristics of a Wing with Quarter-Chord Line Swept Back 35°, Aspect Ratio 4, Taper Ratio 0.6, and NACA 65A006 Airfoil Section. Transonic-Bump Method. NACA RM L9B25, 1949.

3. King, Thomas J., Jr., and Myers, Boyd C., II: Aerodynamic Characteristics of a Wing with Quarter-Chord Line Swept Back 60°, Aspect Ratio 4, Taper Ratio 0.6, and NACA 65A006 Airfoil Section. Transonic-Bump Method. NACA RM L9G27, 1949.

4. Schneiter, Leslie E., and Ziff, Howard L.: Preliminary Investigation of Spoiler Lateral Control on a 42° Sweptback Wing at Transonic Speeds. NACA RM L7F19, 1947.

5. DeYoung, John: Theoretical Additional Span Loading Characteristics of Wings with Arbitrary Sweep, Aspect Ratio, and Taper Ratio. NACA TN 1491, 1947.

6. Multhopp, H: Aerodynamics of the Fuselage. NACA TM 1036, 1942.

CONFIDENTIAL

TABLE I.- FUSELAGE ORDINATES

[Basic fineness ratio 12; actual fineness ratio 10 achieved by cutting off the rear one-sixth of the body; $\bar{c}/4$ located at $l/2$]

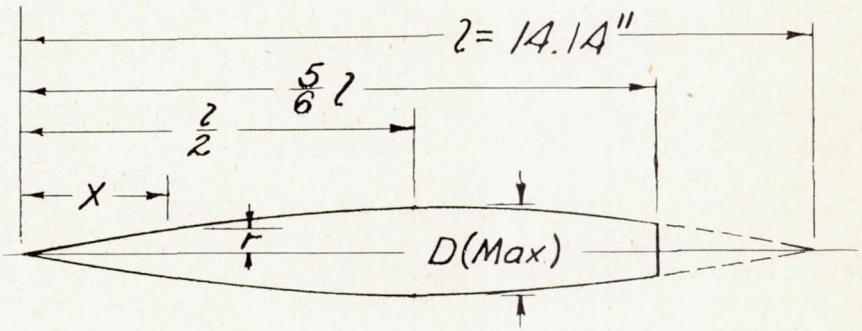

Ordinates			
x/l	r/l	x/l	r/l
0	0		
.005	.00231	.4500	.04143
.0075	.00298	.5000	.04167
.0125	.00428	.5500	.04130
.0250	.00722	.6000	.04024
.0500	.01205	.6500	.03842
.0750	.01613	.7000	.03562
.1000	.01971	.7500	.03128
.1500	.02593	.8000	.02526
.2000	.03090	.8338	.02000
.2500	.03465	.8500	.01852
.3000	.03741	.9000	.01125
.3500	.03933	.9500	.00439
.4000	.04063	1.0000	0
L. E. radius = 0.0005l			

NACA

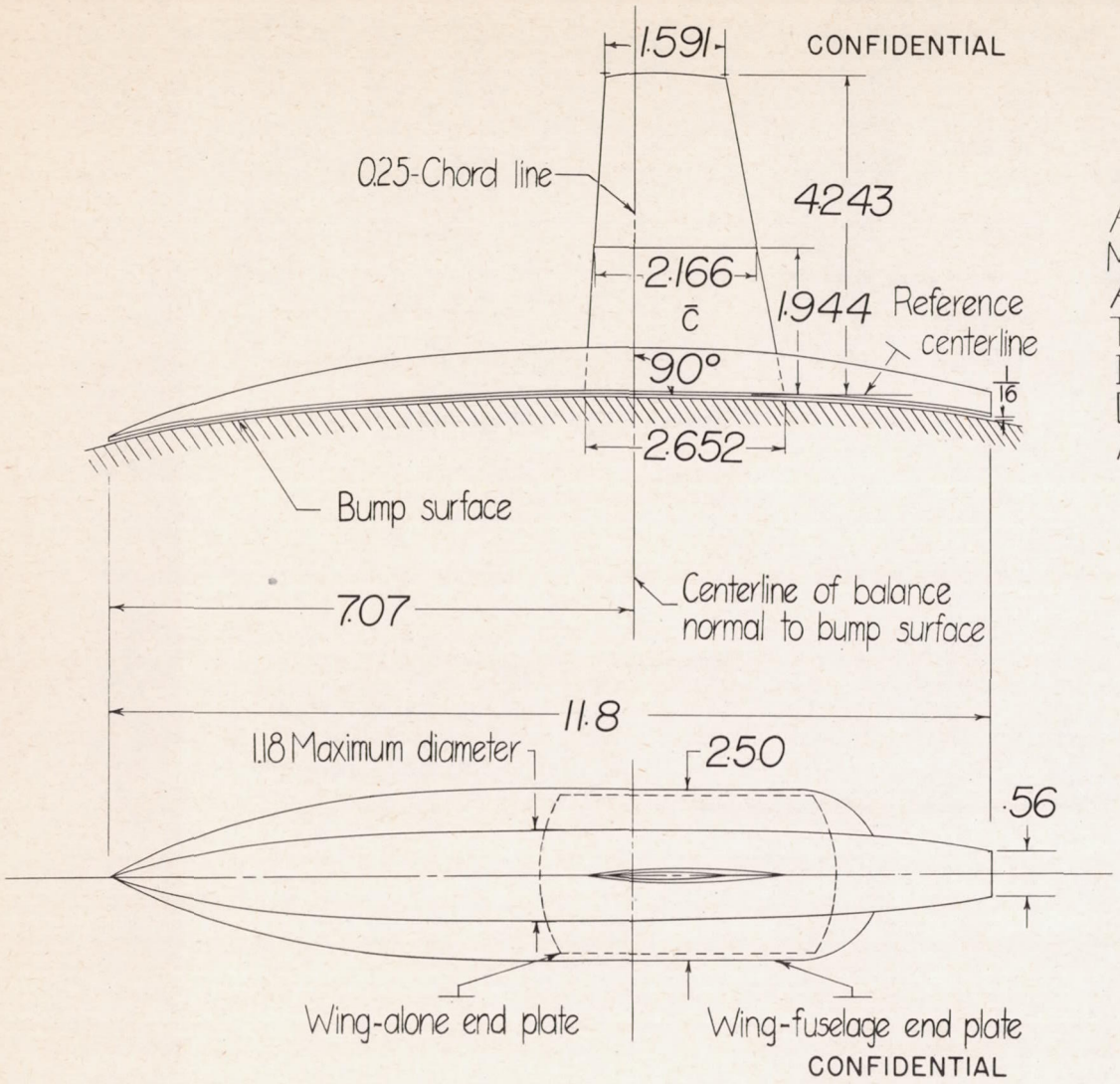

Tabulated Wing Data

Area (Twice semispan)	0.125 sq ft
Mean aerodynamic chord	0.1805 ft
Aspect ratio	4
Taper ratio	0.6
Incidence	0.0°
Dihedral	0.0°
Airfoil section parallel to free stream	NACA 65A006

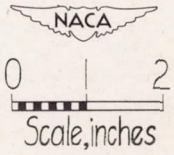

Figure 1.– General arrangement of a model with 0° sweptback wing, aspect ratio 4, taper ratio 0.6, and NACA 65A006 airfoil section.

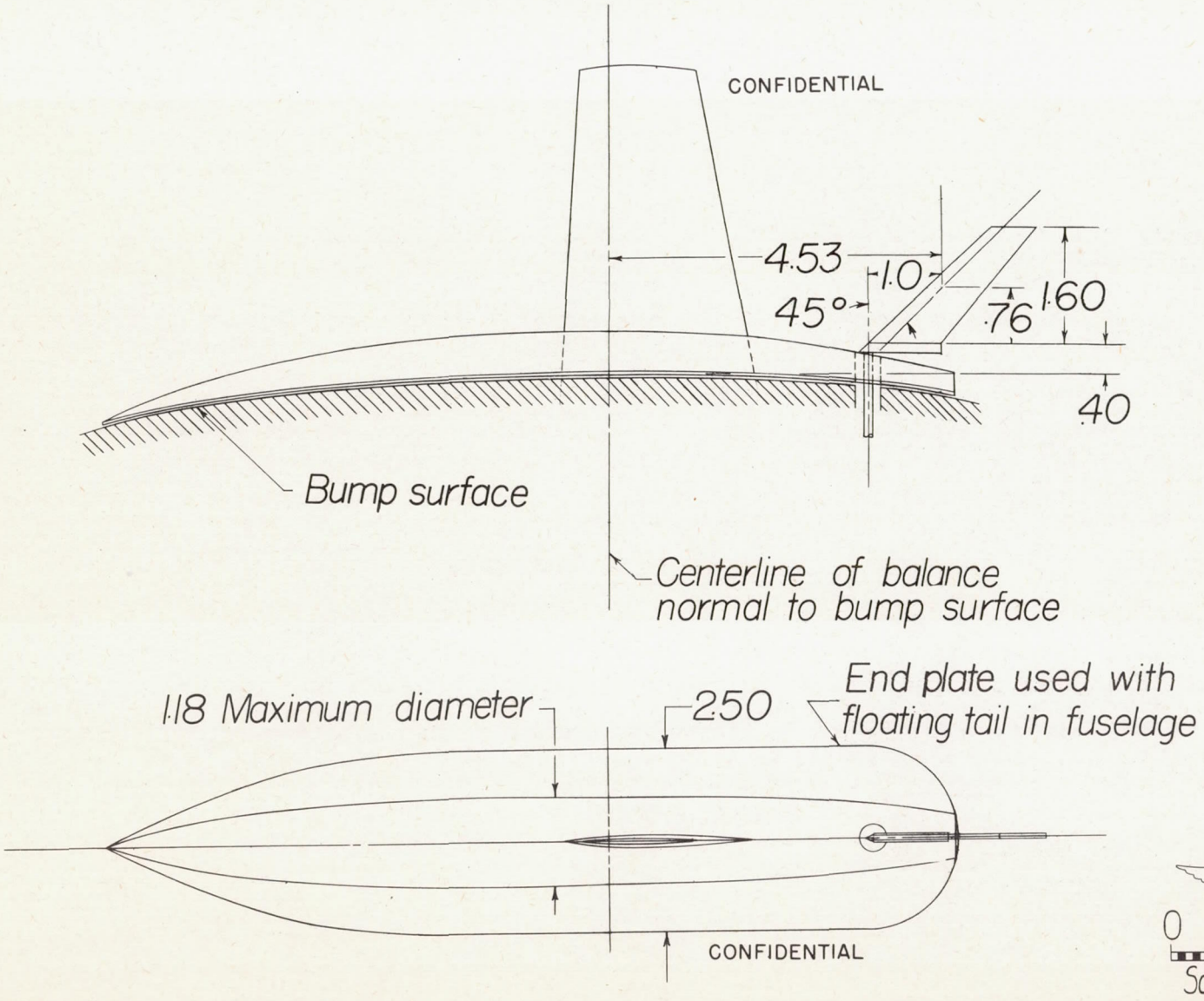

Figure 2.– Details of free-floating tail mounted in fuselage of a model with 0° sweptback wing, aspect ratio 4, taper ratio 0.6, and NACA 65A006 airfoil section.

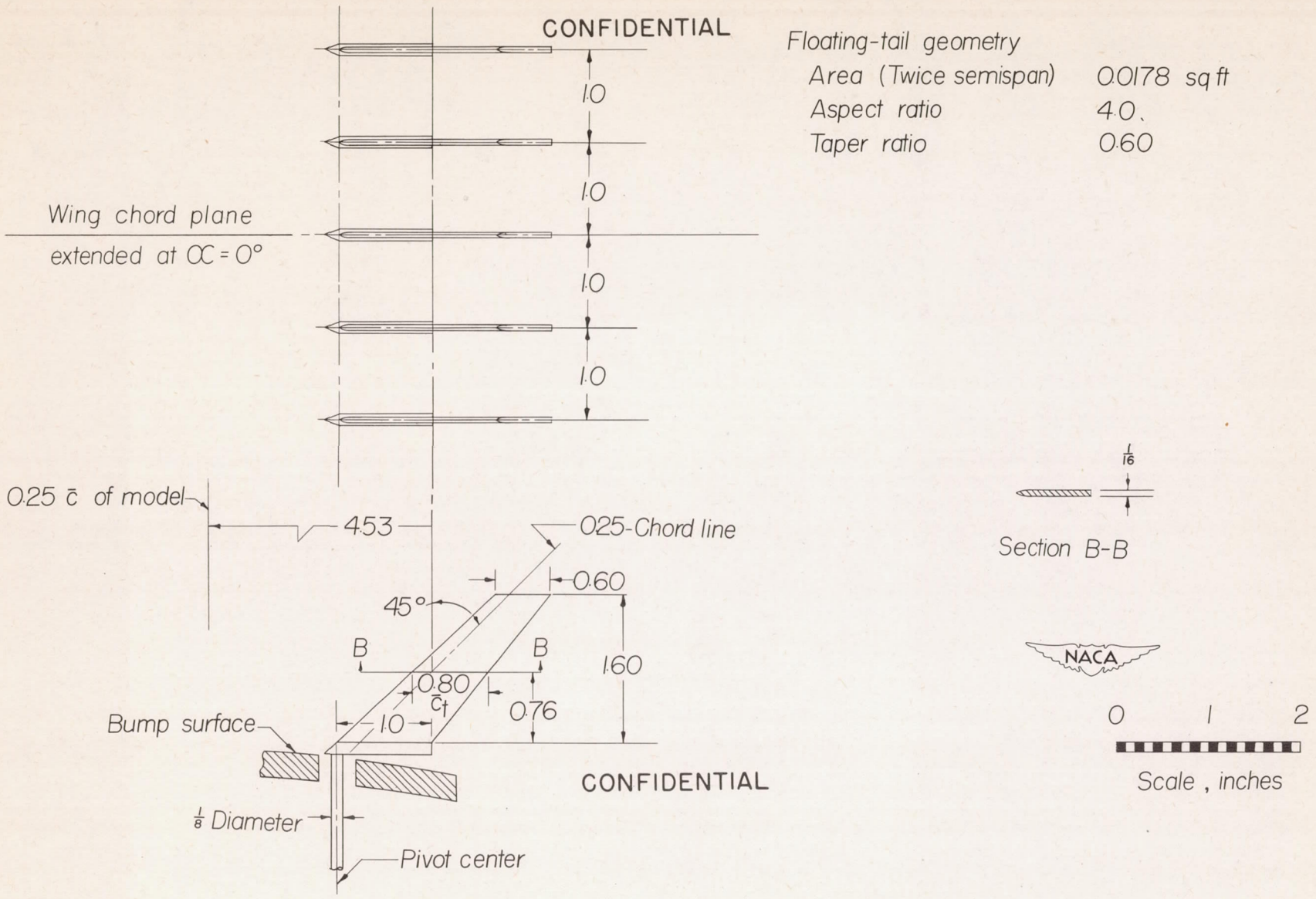

Figure 3.– Details of free–floating tails used in surveys behind model with 0° sweptback wing, aspect ratio 4, taper ratio 0.6, and NACA 65A006 airfoil section.

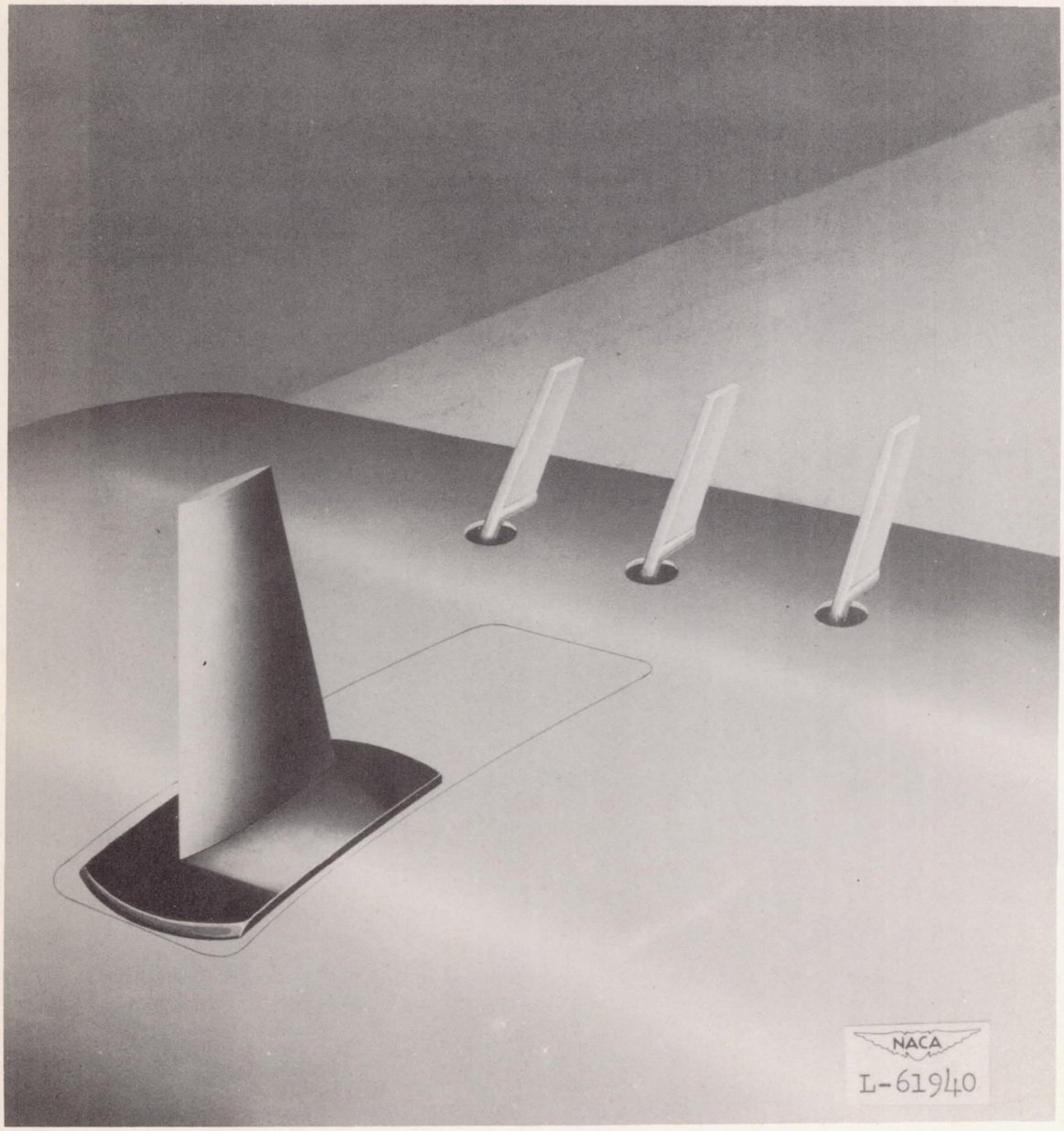

Figure 4.– A pictorial view of a 0° sweptback wing, aspect ratio 4, taper ratio 0.6, and NACA 65A006 airfoil section showing free–floating tails. CONFIDENTIAL

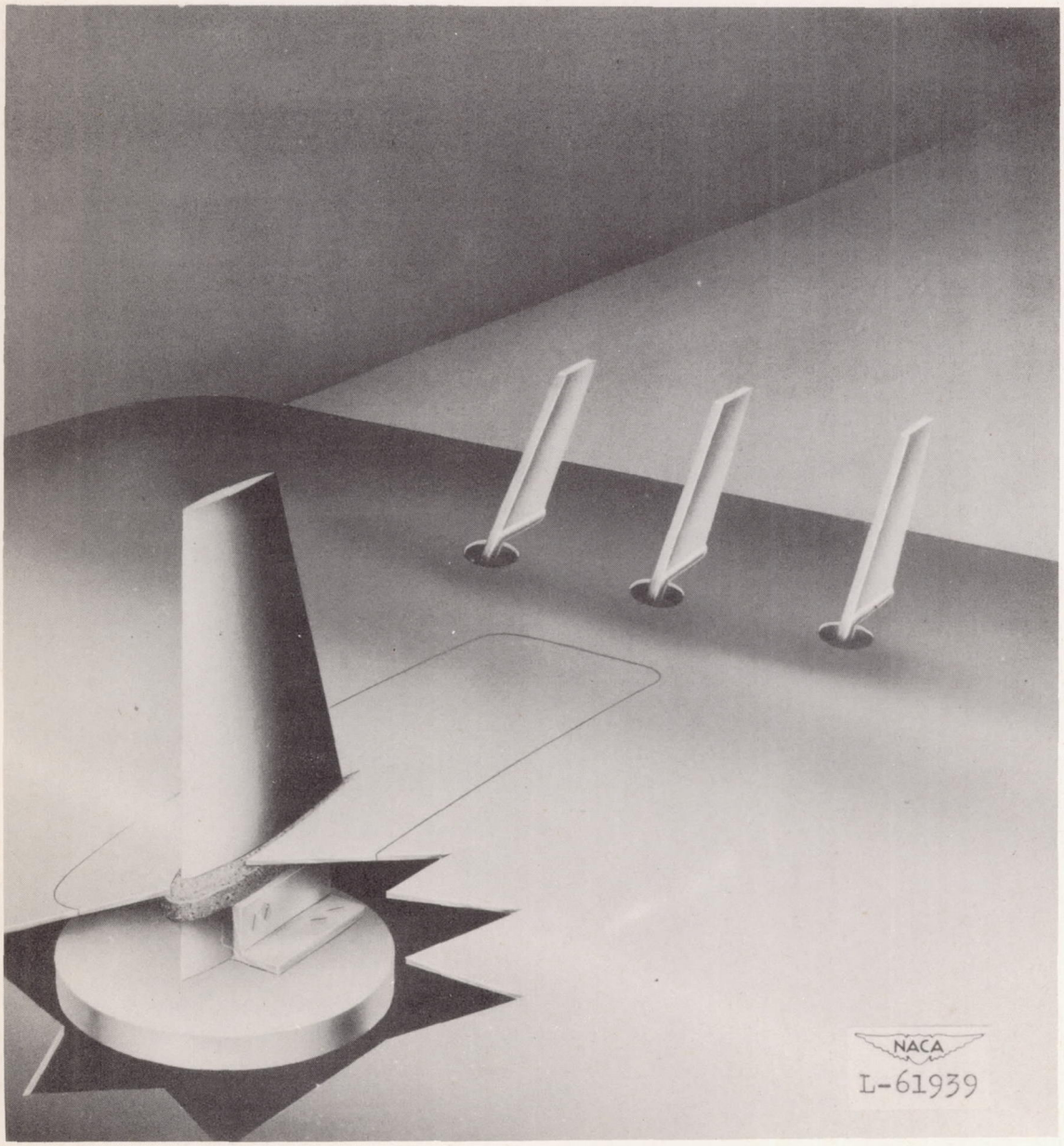

Figure 5.– A pictorial view showing sponge–wiper–seal installation on the model with 0° sweptback wing, aspect ratio 4, taper ratio 0.6, and NACA 65A006 airfoil section.

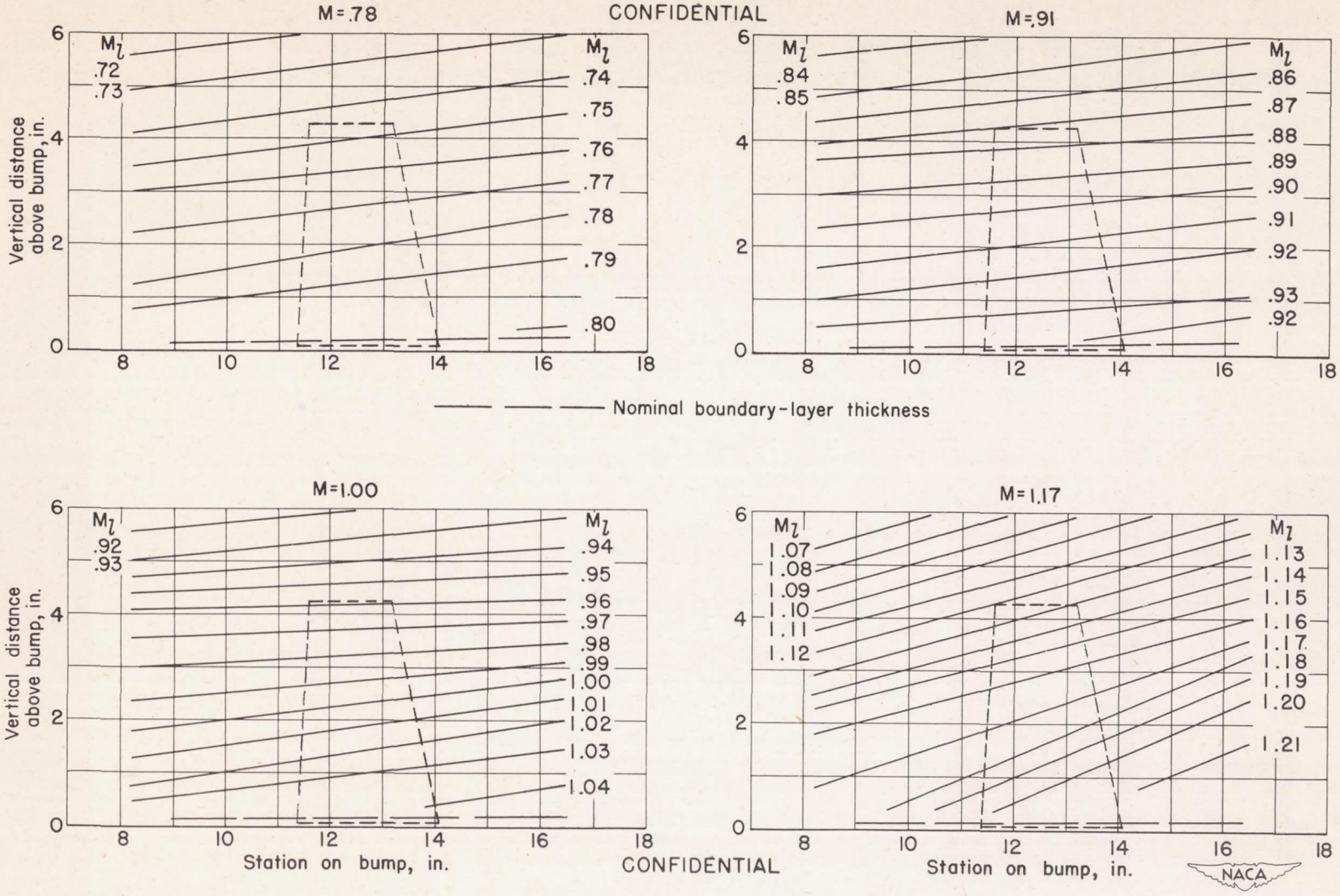

Figure 6.– Typical Mach number contours over transonic bump in region of model location.

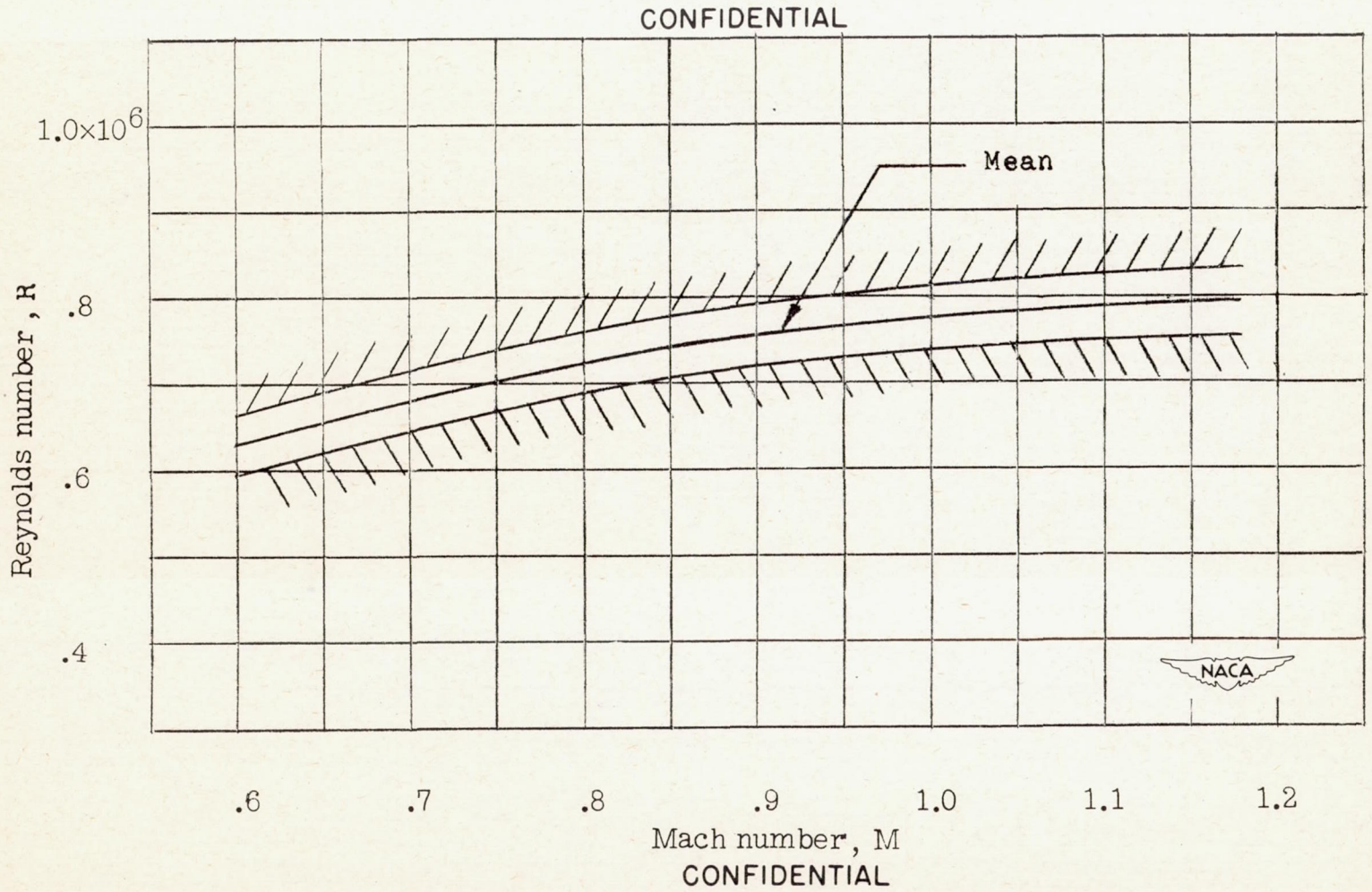

Figure 7.– Variation of test Reynolds number with Mach number for a model with 0° sweptback wing, aspect ratio 4, taper ratio 0.6, and NACA 65A006 airfoil section.

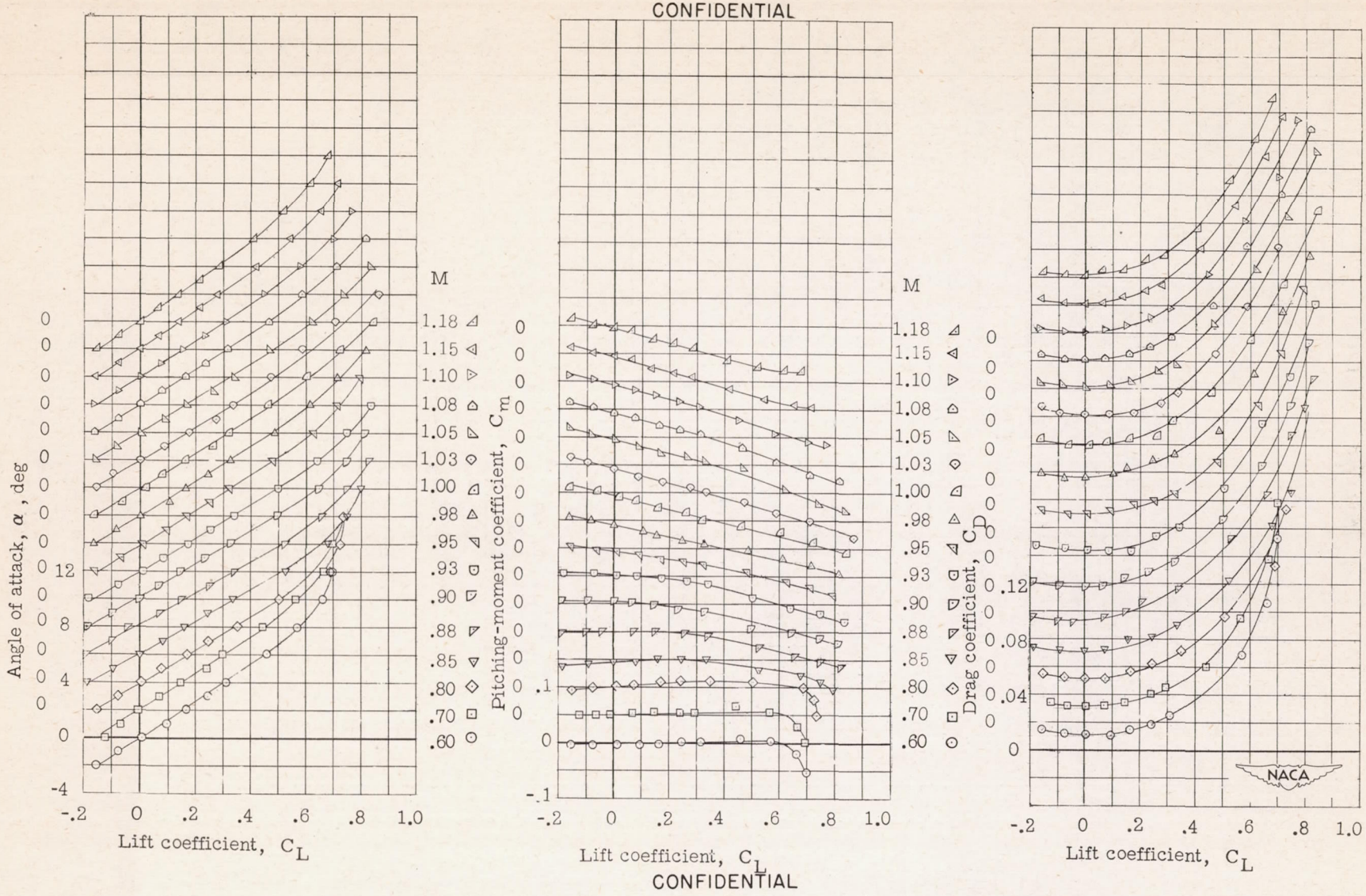

Figure 8.– Aerodynamic characteristics for a model with 0° sweptback wing, aspect ratio 4, taper ratio 0.6, and NACA 65A006 airfoil section. Wing alone.

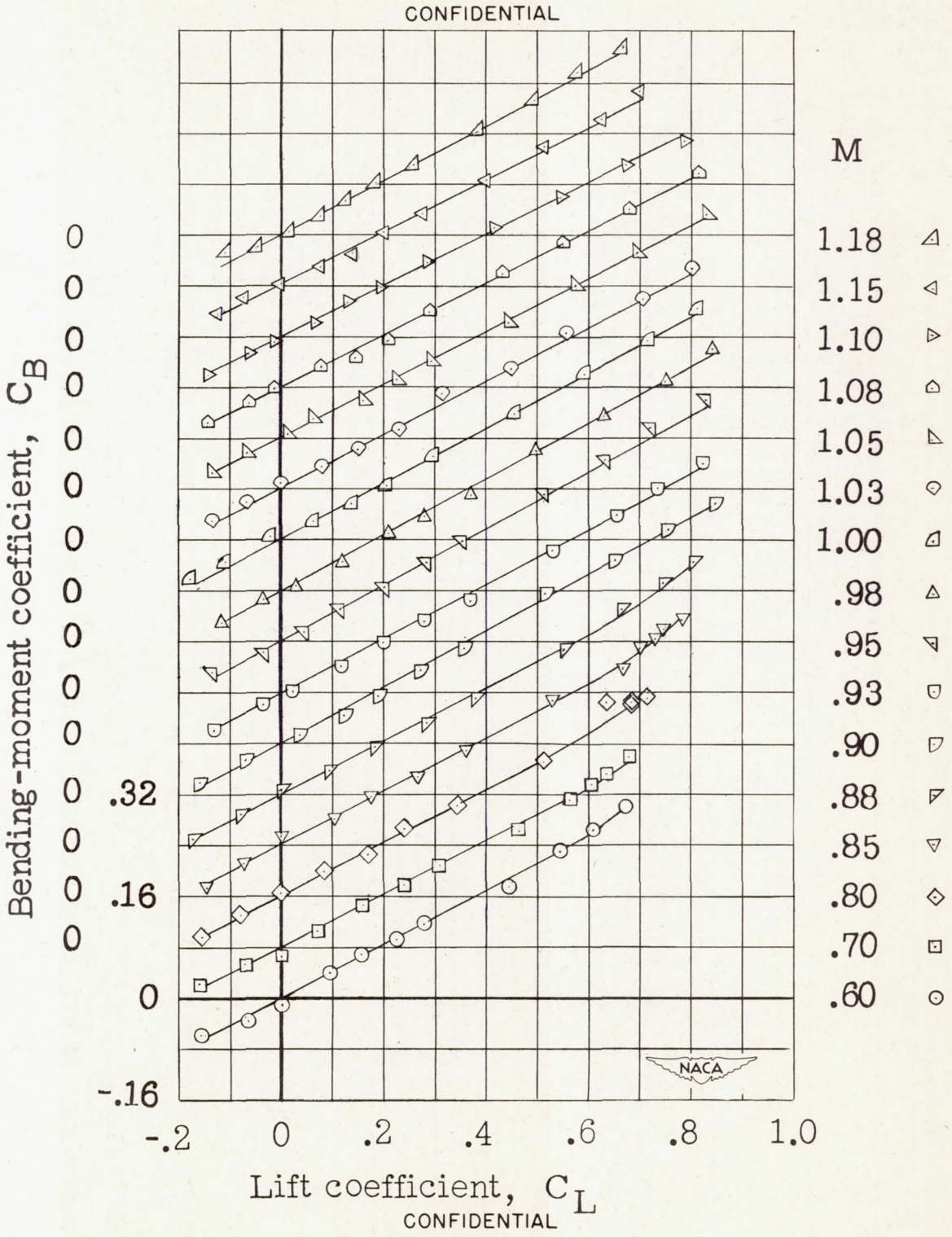

Figure 8.– Concluded.

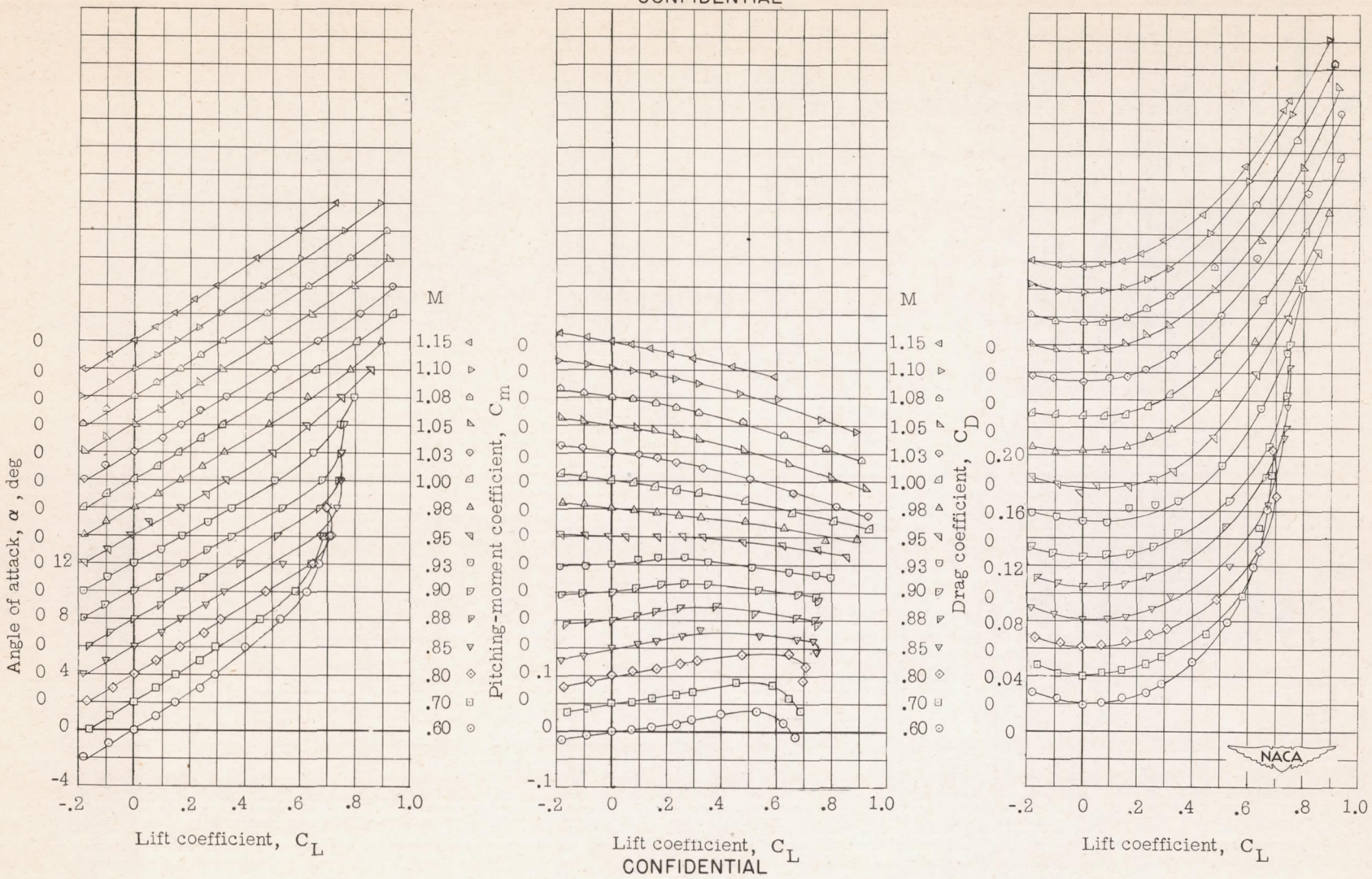

Figure 9.– Aerodynamic characteristics for a model with 0° sweptback wing, aspect ratio 4, taper ratio 0.6, and NACA 65A006 airfoil section. Wing–fuselage.

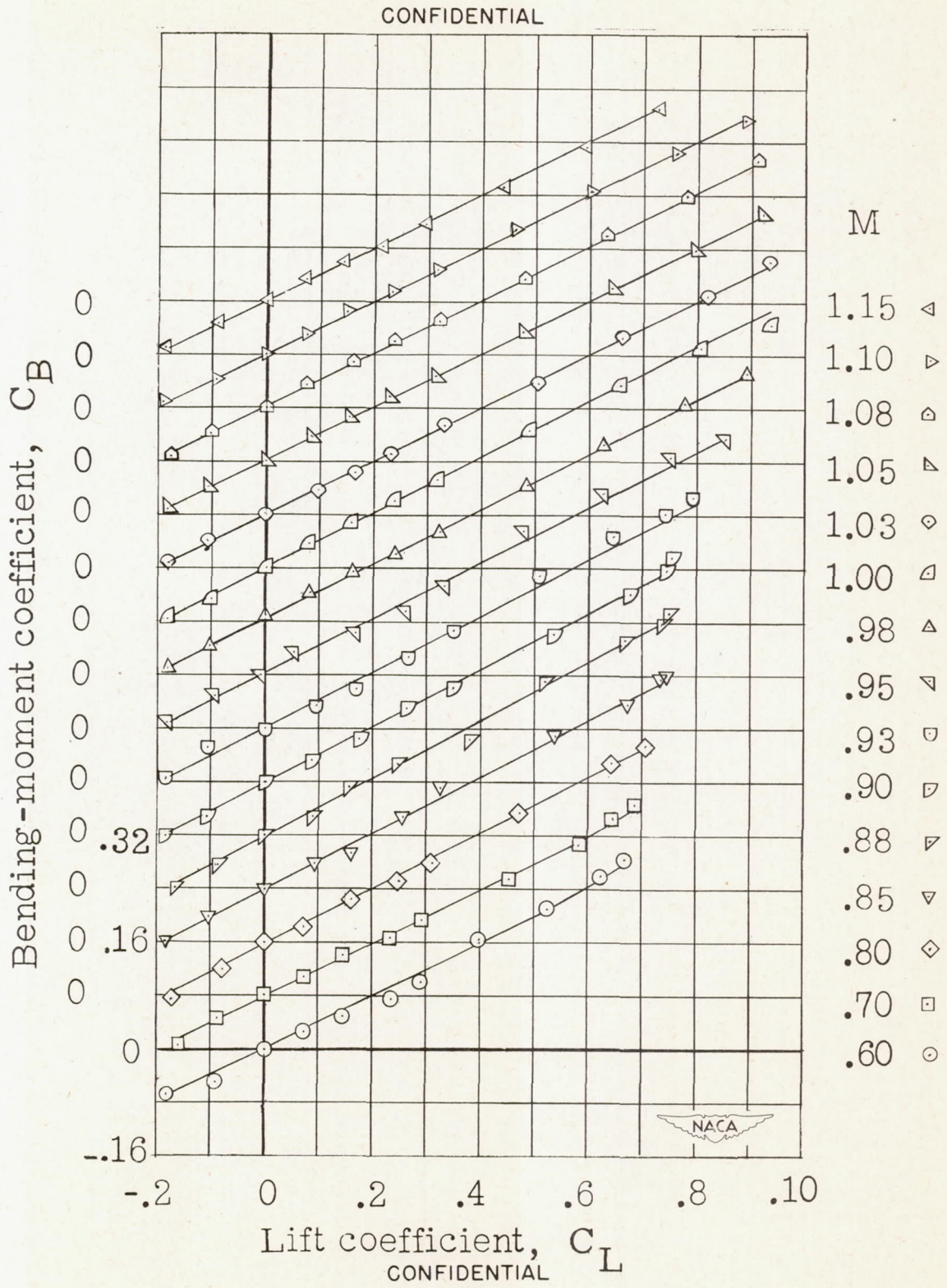

Figure 9.- Concluded.

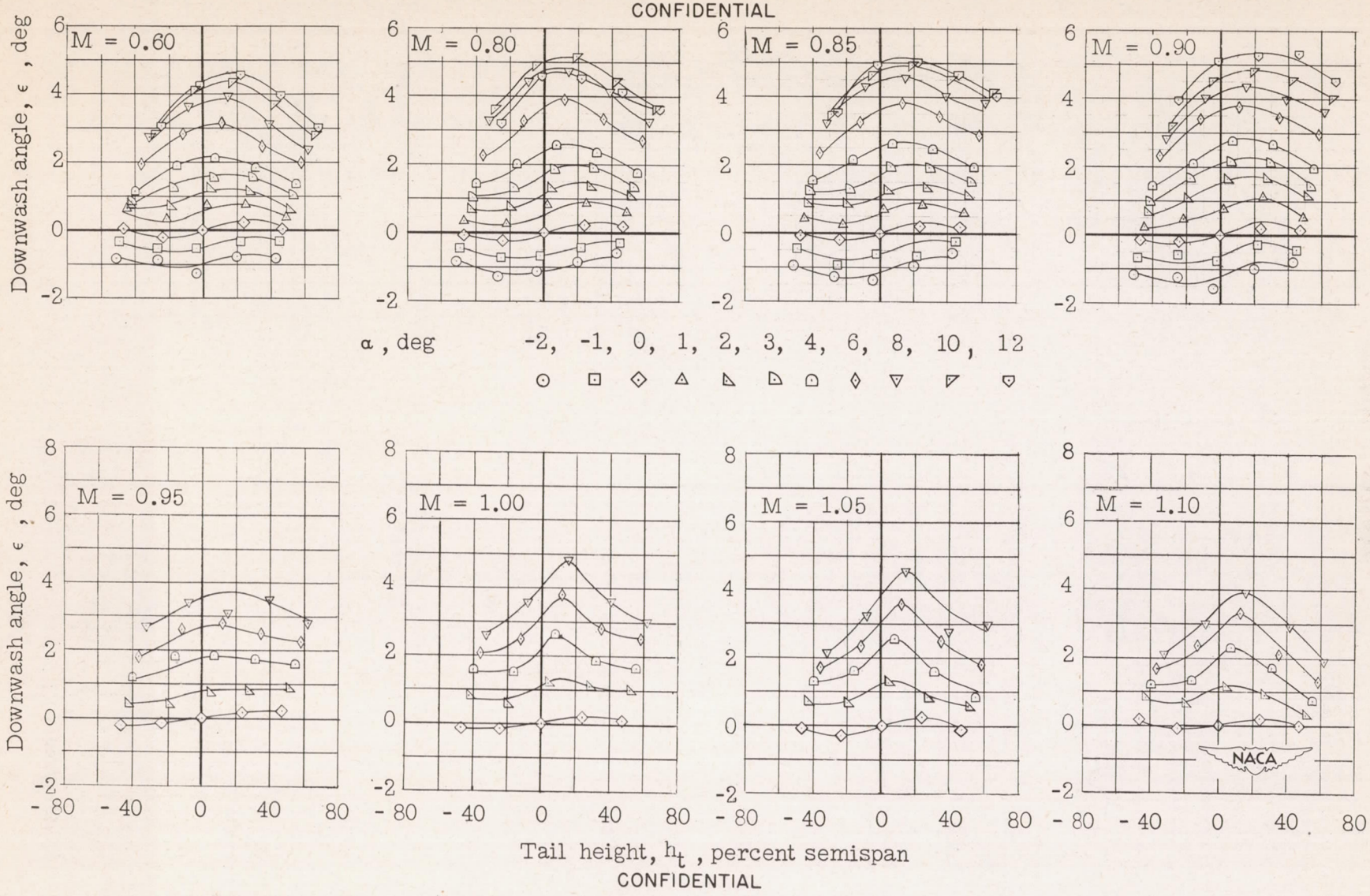

Figure 10.– Effective downwash angles in region of tail plane for a model with 0° sweptback wing, aspect ratio 4, taper ratio 0.6, and NACA 65A006 airfoil section. Wing alone.

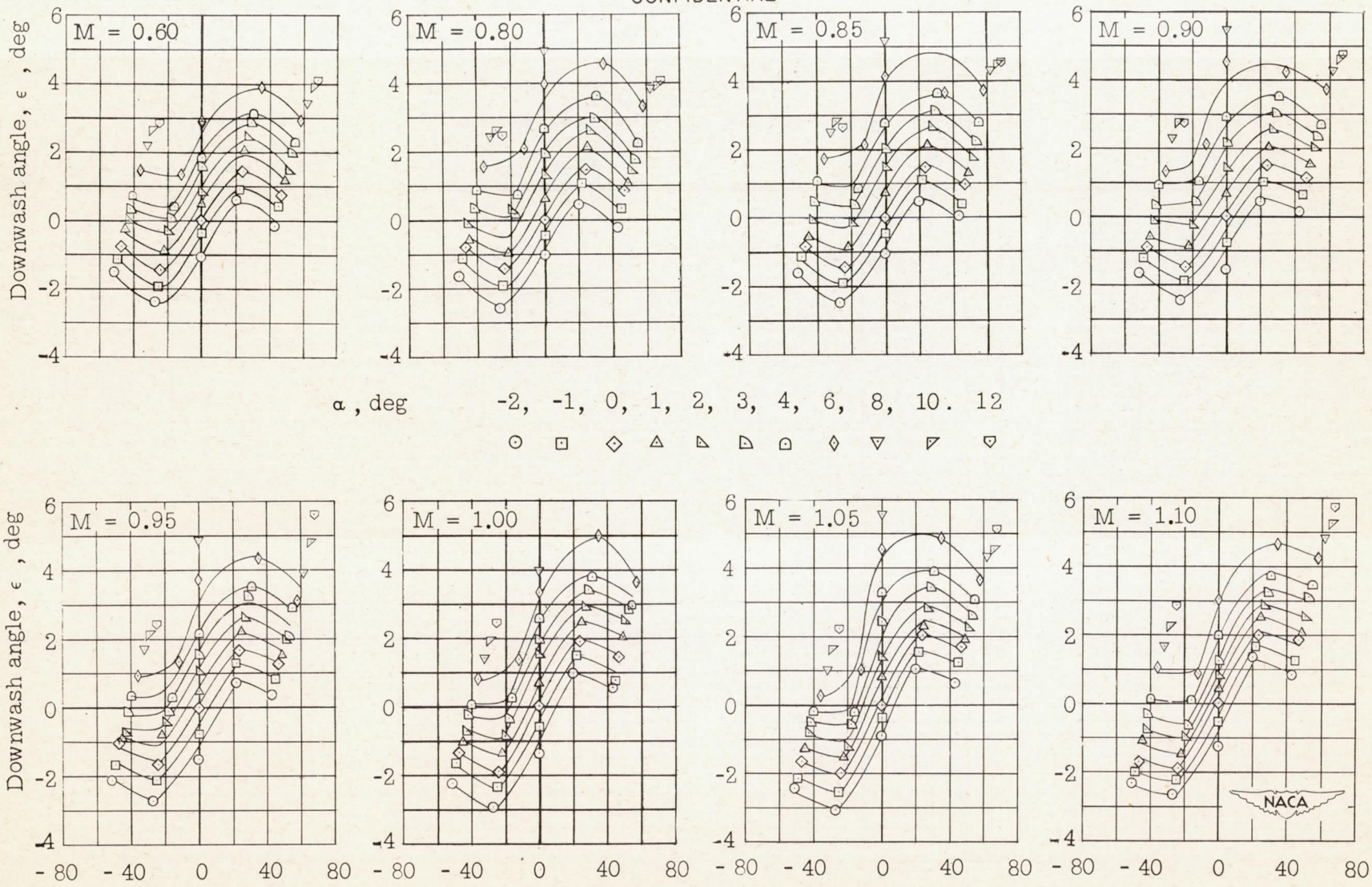

Figure 11.– Effective downwash angles in region of tail plane for a model with 0° sweptback wing, aspect ratio 4, taper ratio 0.6, and NACA 65A006 airfoil section. Wing–fuselage.

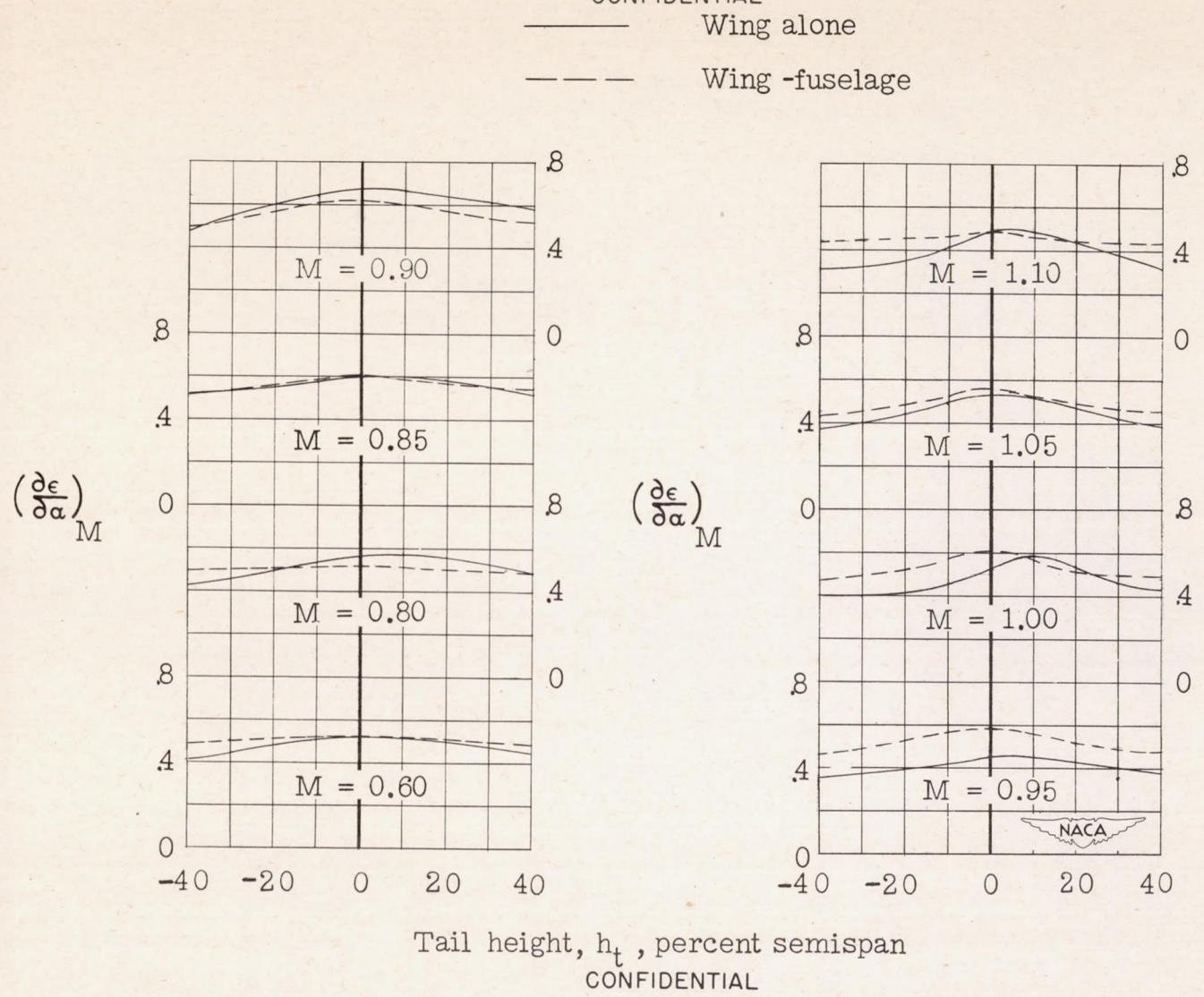

Figure 12.– Variation of downwash gradient with tail height and Mach number for a model with 0° sweptback wing, aspect ratio 4, taper ratio 0.6, and NACA 65A006 airfoil section.

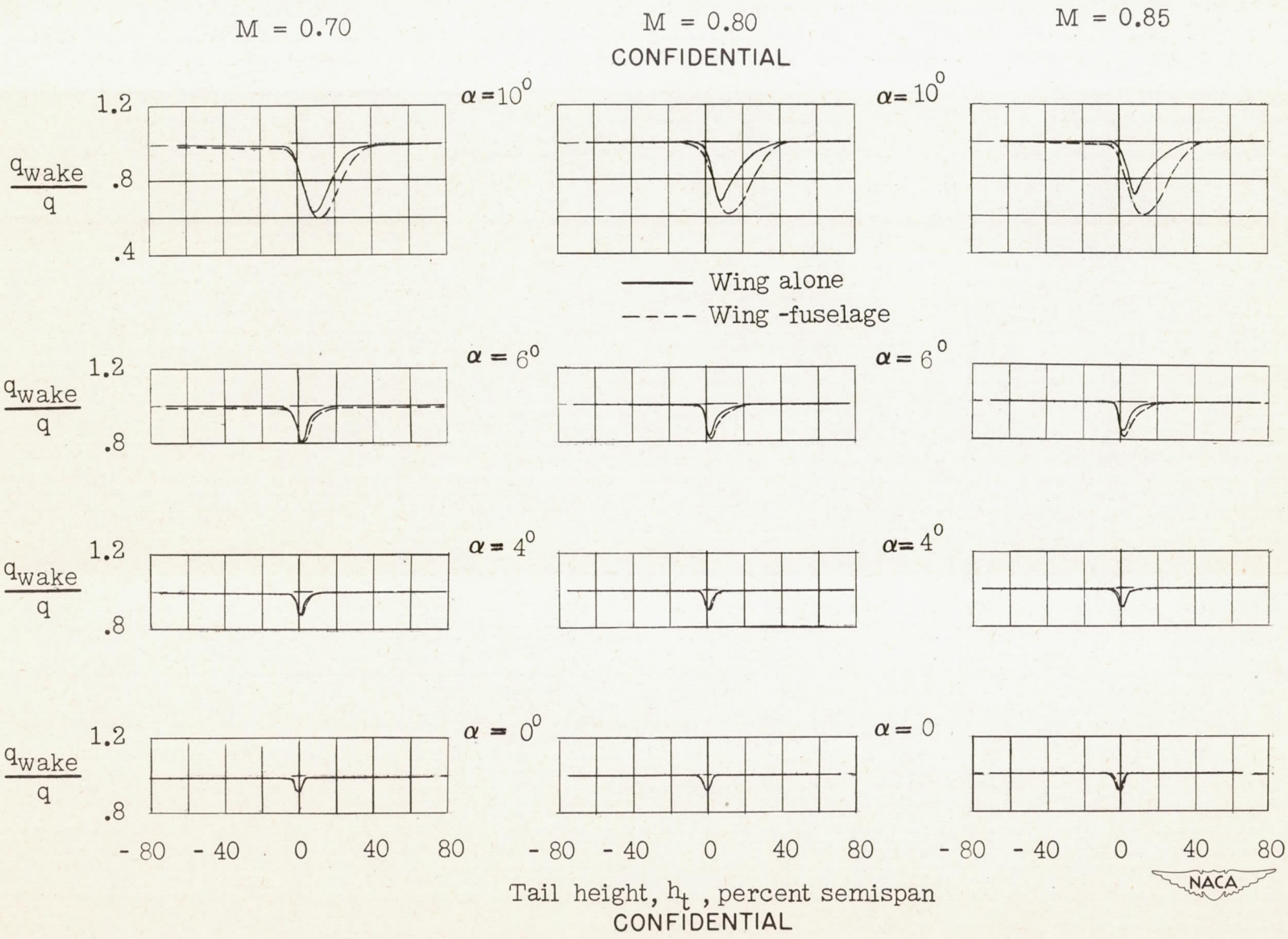

Figure 13.– Dynamic–pressure surveys in region of tail plane for a model with 0° sweptback wing, aspect ratio 4, taper ratio 0.6, and NACA 65A006 airfoil section.

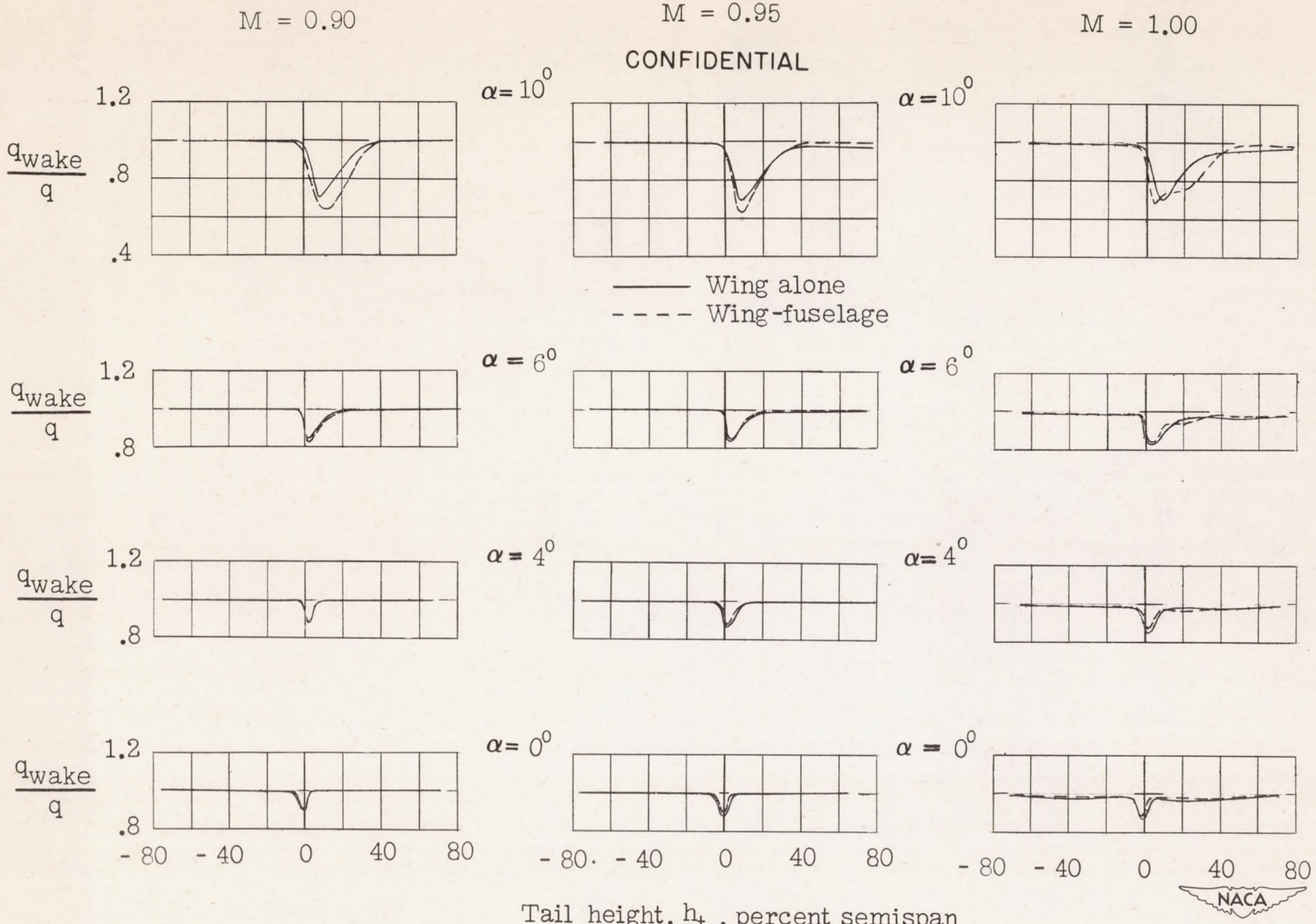

Figure 13.– Continued.

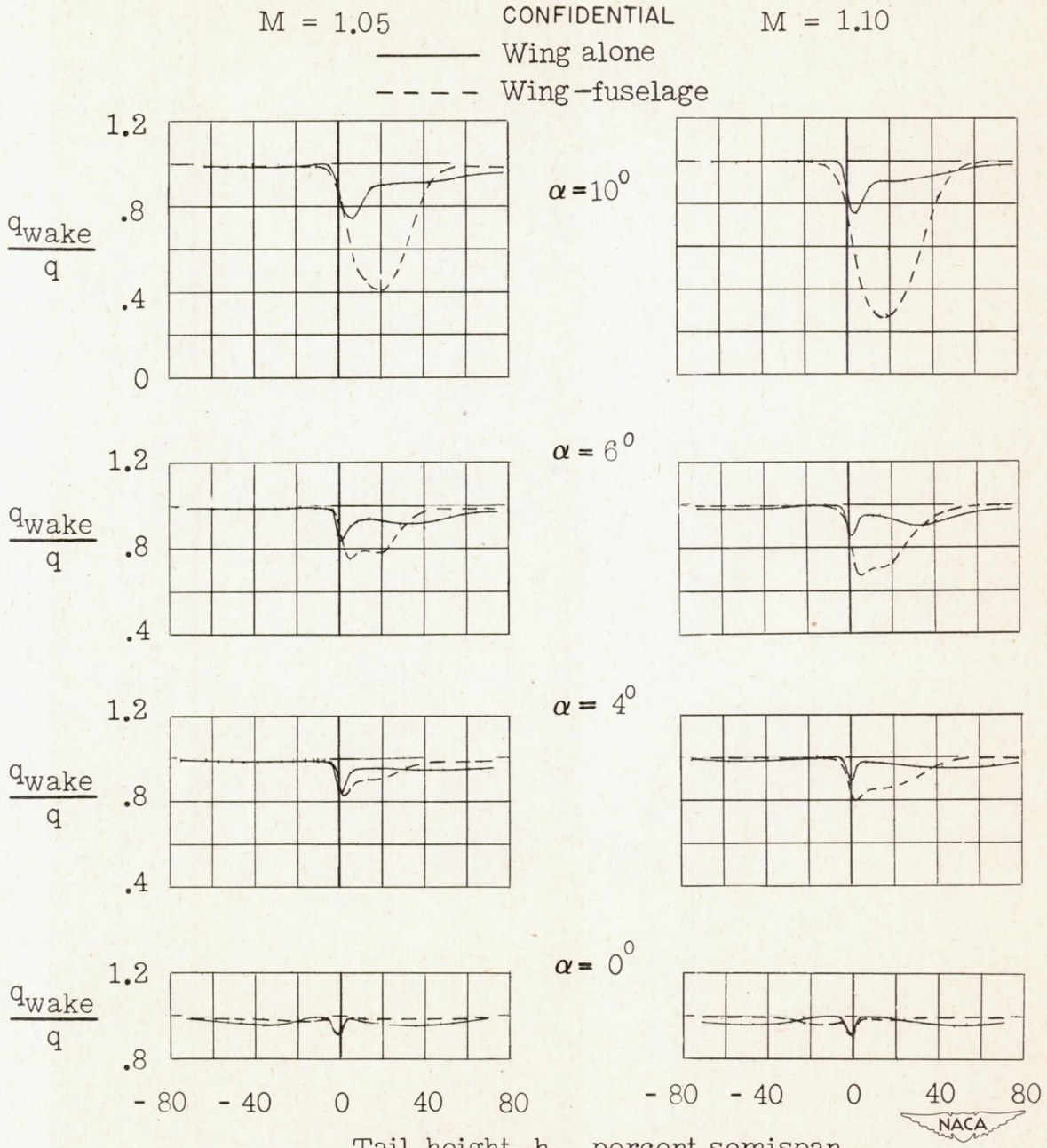

Figure 13.– Concluded.

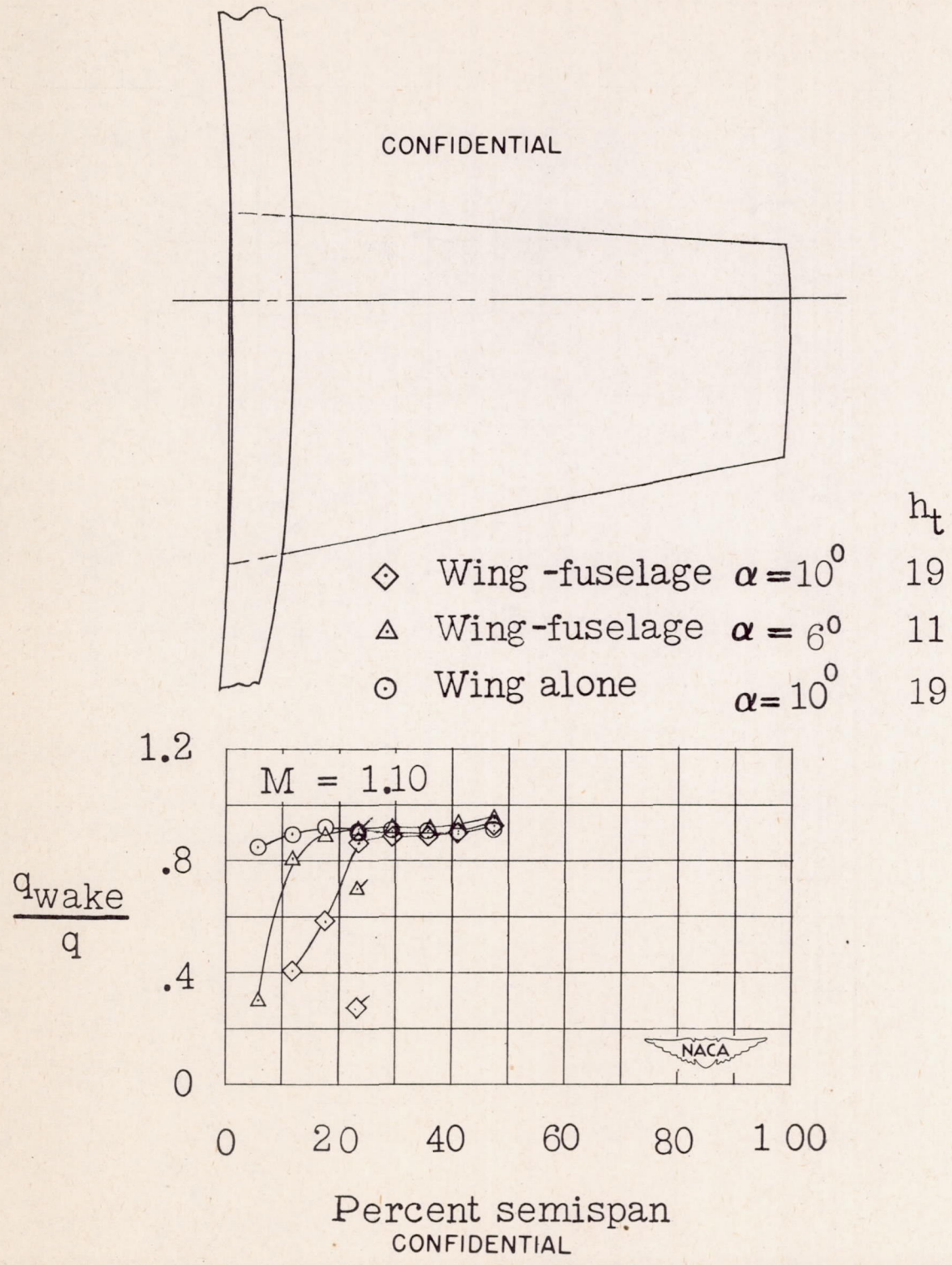

Figure 14.– Spanwise dynamic-pressure surveys in region of tail plane for a model with 0° sweptback wing, aspect ratio 4, taper ratio 0.6, and NACA 65A006 airfoil section.

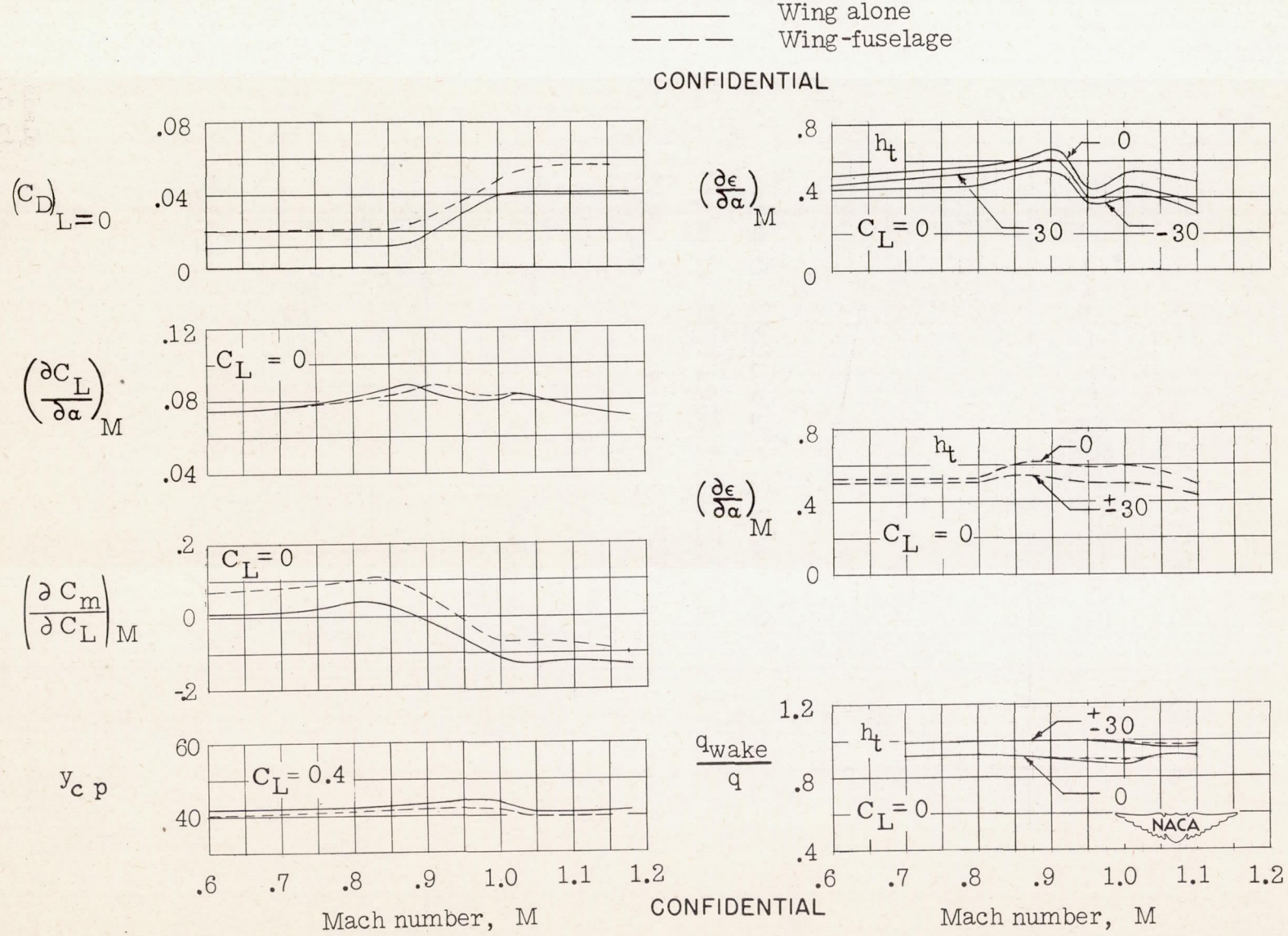

Figure 15.– Summary of aerodynamic characteristics for a model with 0° sweptback wing, aspect ratio 4, taper ratio 0.6, and NACA 65A006 airfoil section.

NACA-Langley - 10-21-49 - 400